Lab on a Chip

Accepted Manuscript

This is an *Accepted Manuscript*, which has been through the Royal Society of Chemistry peer review process and has been accepted for publication.

Accepted Manuscripts are published online shortly after acceptance, before technical editing, formatting and proof reading. Using this free service, authors can make their results available to the community, in citable form, before we publish the edited article. We will replace this *Accepted Manuscript* with the edited and formatted *Advance Article* as soon as it is available.

You can find more information about *Accepted Manuscripts* in the Information for Authors.

Please note that technical editing may introduce minor changes to the text and/or graphics, which may alter content. The journal's standard Terms & Conditions and the Ethical guidelines still apply. In no event shall the Royal Society of Chemistry be held responsible for any errors or omissions in this *Accepted Manuscript* or any consequences arising from the use of any information it contains.

ROYAL SOCIETY OF CHEMISTRY

www.rsc.org/loc

Microfluidic Pumping, Routing and Metering by Contactless Metal-Based Electro-osmosis

Xiaotong Fu
Nicholas Mavrogiannis
Steven Doria
Zachary Gagnon
Johns Hopkins University, Department of Chemical and Biomolecular Engineering
Maryland Hall 220A

Corresponding Author:

Zachary Gagnon
Johns Hopkins University
3400 North Charles St.
Maryland Hall 220A
Baltimore MD 21218
zgagnon1@jhmi.edu

Lab on a Chip Accepted Manuscript

Abstract

Over the past decade, many microfluidic platforms for fluid processing have been developed in order to perform on-chip fluidic manipulations. Many of these methods, however, require expensive and bulky external supporting equipment, which are not typically applicable for microsystems requiring portability. We have developed a new type of portable contactless metal electro-osmotic micropump capable of on-chip fluid pumping, routing and metering. The pump operates using two pairs of gallium metal electrodes, which are activated using an external voltage source, and separated from a main flow channel by a thin micron-scale PDMS membrane. The thin contactless membrane allows for field penetration and electro-osmotic (EO) flow within the microchannel, but eliminates electrode damage and sample contamination commonly associated with traditional DC electro-osmostic pumps that utilize electrodes in direct contact with the working fluid. The maximum flow rates and pressures generated by the pump using DI water as a working buffer are 10 nL/min and 30 Pa, respectively. With our current design, the maximum operational conductivity where fluid flow is observed is 0.1 mS/cm. Due to the small size and simple fabrication procedure, multiple micropump units can be integrated into a single microfluidic device for automated on-chip routing and sample metering applications. We experimentally demonstrated the ability to quantify micropump electro-osmotic flowrate and pressure as a function of applied voltage, and developed a mathematical model capable of predicting the performance of a contactless micropump for a given external load and internal hydrodynamic microchannel resistance. Finally, we showed that by activating specific pumps within a microchannel network, our micropumps are capable of routing microchannel fluid flow and generating plugs of solute.

Lab on a Chip Accepted Manuscript

Microfluidic Pumping by Contactless Metal-Based Electro-osmosis

1. Introduction

The development of robust and portable microfluidic platforms capable of performing complex fluidic routing and handling operations without external laboratory equipment is an important requirement for the next generation of portable micro total analysis systems (μTAS, or lab-on-a-chip).[1] Many microfluidic platforms are capable of performing on-chip fluidic pumping[2], valving[3], mixing[4] and routing.[5] A popular method, known as microfluidic large-scale integration (LSI)[6], for example, utilizes thousands of integrated pressure-actuated elastomeric pumps and valves to handle fluidic operations. Another platform uses centrifugal forces to drive fluid flow within a network of microchannels valves situated atop a rotating microfluidic disk.[7] Others have used on-chip surface acoustic waves[8] and electrical forces[9] to perform on-chip fluidic operations. The past two decades in particular have demonstrated the effectiveness of these and other microfluidic platforms as enabling systems for performing fluid routing, mixing, and pumping for applications including nucleic acid extraction[10], protein crystallization[11], immunoassays[12], single cell analysis[13], and high throughput genetic screening.[14] The majority of these platforms, however, require large supporting equipment, which confine their usefulness to the laboratory, and are typically too large and expensive for use in portable environments, rural areas, and for general use by consumers. Applications suited for use in more portable settings (e.g. point-of-care diagnostics) are limited due to the lack of robust and portable microfluidic platforms. The development of microfluidic lab-on-a-chip (LOC) systems that are capable of performing fluidic-based unit operations is therefore an important aspect of microfluidic research. Progress in this area is

Lab on a Chip Accepted Manuscript

largely limited due to inherent difficulties in performing desired tasks, such as fluid pumping and metering, without the need for large external driving systems. In terms of developing portable microfluidic systems for diagnostics, personalized medicine, and environmental monitoring, fluid manipulation technology is a central bottleneck in reaching this goal.

Micro-pumps can be generally divided into two categories: displacement pumps and kinetic pumps.[15] Displacement pumps, also known as mechanical pumps, utilize moving parts such as membranes and valves to induce fluid flow. At the microscale, however, they often suffer from mechanical failure due to fouling or loss in membrane elasticity.[16] Kinetic pumps convert kinetic sources such as electromagnetic, thermal or chemical energy into fluid momentum to drive flow. Common types of kinetic pumps include electrohydrodynamic[17], electrokinetic[18], magnetohydrodynamic[19], thermomagnetic[20], electro wetting[21], electrothermal[22], and electrochemical.[23]

Electrokinetic pumps in particular use electrical forces to induce electro-osmotic (EO) fluid flow and offer a popular alternative to mechanical displacement micropumps. Typically, however, EO pumps require direct contact between electric field-generating electrodes and a working fluid. When a direct current (DC) voltage is applied, Faradaic reactions occur at each electrode surface, which can lead to uncontrolled electrothermal fluid flow[24], electrode damage, and sample damage[25] from pH generation[26] and Joule heating.[27] Alternating current (AC) electro-osmotic pumps have been developed to alleviate some of these drawbacks. AC EO pumps do not suffer from Faradaic reactions, and are capable of pumping low conductivity aqueous electrolytes in microchannels.[28,29] However, they require large microelectrode arrays, which are expensive and time consuming to fabricate.

Recently, a new type of contactless electrode device was developed for use

Lab on a Chip Accepted Manuscript

in dielectrophoresis (DEP) by Sano et al.[30] In contactless DEP (cDEP), two conductive electrolyte channels serve as liquid electrodes, which are physically isolated from the main flow channel by a thin PDMS membrane. The application of an AC or DC voltage source across the liquid electrodes allows for electric field penetration through the membrane and into the main flow channel. This contactless approach eliminates Faradaic reactions and buffer contamination issues associated with traditional metal electrode systems, and has been successfully used for dielectrophoretic particle and cell sorting, and very recently demonstrated for microchannel electro-osmosis.[30] Currently, however, these contactless devices have been based on external liquid electrodes. While effective, liquid electrodes lack the required features necessary for creating a portable microfluidic platform. First, they can suffer from evaporation and cannot be reliably transported. Second, liquid electrodes require fluid injection ports and pipette tips to maintain electrical contact, and inherently posses a large operational footprint, which currently limits the number of active devices that can be effectively fabricated on a single chip.

Here, we present a new type of contactless direct current (DC) micropump for on-chip liquid pumping, routing, and metering that has the potential of being developed into a portable microfluidic fluid-handling platform. Instead of using liquid electrodes, our micropump design is based on 3D gallium metal electrodes fabricated directly into the sidewalls of microfluidic flow channels, and separated from the active flow region by a thin micron-scale PDMS polymer membrane (Fig 1a). To create an electric field within the main microchannel, two different voltages are applied to each electrode pair (V_1 and V_2). At a sufficiently large voltage (> 650 V), an electric field penetrates the resistive PDMS membrane and drives an electro-osmotic flow within the flow channel. In terms of more portable fluid pumping and routing, the presented metal-based electrode design is a

Lab on a Chip Accepted Manuscript

significant improvement over existing contactless electrokinetic devices that utilize liquid electrolyte electrodes. Most importantly, unlike liquid-based electrode designs, our metal-based contactless approach is scalable. We demonstrate the ability to fabricate and independently operate multiple micropumps on a single microfluidic device for fluid pumping, routing, and metering. With the ability to activate and route fluid flow at different pumping locations on-chip independently over a microfluidic network, it is important to understand how to characterize and measure the contactless pump working capacity. With this in mind, we present two different microfluidic channel designs – a closed microfluidic circulating "loop" (Fig. 2a) and a "T-shape" channel (Fig. 2b) – with supporting theoretical pumping models to quantify the contactless pump pressure and flow rate under varying hydrodynamic loads. The closed circuit "Loop" is used to measure the flow rate in a fluid network with a known hydrodynamic resistance, which simulates microchannel systems solely driven by internal micropumps. Alternatively, the "T-shape" channel design is used to measure the pump capability at maximum pressure.

The first part of this paper is an analysis of contactless electro-osmotic flow within a microchannel. The governing fluid transport equations are formulated and used to derive relations describing electro-osmotic flow rate in the presence of an arbitrary hydrodynamic resistance within a microfluidic network. These equations are then combined with an electrostatic model for our contactless electrode design, and utilized to describe the relation between the applied voltage and the resulting induced electro-osmotic flow. In the second part of this work, electro-osmotic flow rate experiments for two different microfluidic geometries are presented and combined with our contactless micropump model to quantitatively characterize the on-chip micropump. Finally, we demonstrate the usefulness of our gallium contactless micropumps by using them to perform microfluidic fluid

Lab on a Chip Accepted Manuscript

routing and solute plug generation.

2. Theory of Contactless EO Pumping

In this section, we derive the theoretical formulation for electro-osmotic flow within a microfluidic channel and develop equations to relate the applied micropump voltage drop across a set of microchannel electrodes to that of the pressure gradient and flow rate produced by the electro-osmotic pump.

Electro-osmosis is an electrokinetic technique for pumping fluids in microfluidic channels.[31] Solid-liquid surfaces tend to develop surface charge when in contact with aqueous liquids. This surface charge attracts counter-ions of opposite charge and repels co-ions of similar charge, and an electrical double layer (EDL) is formed. The resulting ionic double layer possesses a non-zero charge density and screens the solid surface charge over a characteristic Debye length. When an external electric potential, ϕ, is dropped parallel to the EDL, the ions suffer a Coulombic force and move towards the electrode of opposite polarity. This creates motion of the fluid near the wall and transfers momentum into the bulk fluid. Assuming the applied electric field is uniform inside the EDL, the flow is unidirectional, and there is no external applied pressure gradient, the Stokes equations can be written as

$$0 = \mu \frac{\partial^2 u}{\partial y^2} - \varepsilon \frac{\partial^2 \phi}{\partial y^2} E_{wall}, \qquad (1)$$

where μ, ε, and E_{wall} are the fluid viscosity and electrolyte permittivity, and applied tangential electric field at the channel wall, respectively. In the absence of any external pressure gradient, the flow field within the EDL is adequately described though a balance between viscous stress and electric body force, and Eq. (1) can be integrated with a no slip condition at the wall ($y=0$) and a far-field condition that

Lab on a Chip Accepted Manuscript

$\phi \to 0$ as $y \to \infty$ to give:

$$u_{slip} = \frac{\varepsilon E_{wall}}{\mu}(\phi - \phi_{wall}). \quad (2)$$

Here, the wall potential, $\phi_{wall} = \zeta e^{-y/\lambda_D}$, varies across the Debye length, λ_D, which exponentially approaches a Smoluchowski's slip velocity outside the diffuse layer,

$$u_{EO} = \frac{\varepsilon E_{wall}\zeta}{\mu}, \quad (3)$$

where ζ is the zeta potential at the channel surface. For a channel of width, *w*, and height, *d*, the total electro-osmotic flow rate, Q_{EO}, is calculated by integrating Eq. (3) over the channel cross-section area:

$$Q_{EO} = -2wd\frac{\varepsilon E_{wall}\zeta}{\mu}. \quad (4)$$

For the case where a micropump must drive fluid flow against a hydrodynamic load (e.g. within a network of microchannels), a backpressure is generated and the fluid flow is reduced. A combination of EO flow and this counter backpressure is known as "frustrated" flow[9], and for a slot-shaped microchannel (i.e. the channel width is much larger than the height, *w* >> *2d*) the total frustrated flow rate is a linear combination of EO and pressure driven back flow,

$$Q = \frac{2wd^3}{3\mu}\left[\frac{\partial P}{\partial x}\right] - 2wd\frac{\varepsilon E_{wall}\zeta}{\mu}. \quad (5)$$

Illustrated in Fig. 1a, for a given applied voltage drop, ΔV, dropped over an

Lab on a Chip Accepted Manuscript

electrode separation length, L_E, the electric field at the wall is $\Delta V / L_E$. The back pressure gradient varies linearly along the micropump length, and can be written as $\Delta P / L_E$. The maximum pump pressure can be derived using Eq. (5). Setting $Q=0$, which is the case for a closed microchannel[32], the maximum EO-induced pump pressure can be written as:

$$\Delta P_{\max} = -\frac{3\mu u_{EO}}{d^2}\Delta V . \quad (6)$$

In contrast, the maximum flow rate can be calculated by setting $\Delta P = 0$:

$$Q_{\max} = 2wdu_{EO}\frac{\Delta V}{L_E}. \quad (7)$$

Microfluidic channel designs that either of these two extreme cases are rare; neither the pressure nor net flow rate are zero. Combining Eqs. (5-7), a relation linking pumping flow rate and pressure is obtained:

$$\frac{\Delta P}{\Delta P_{\max}} + \frac{Q}{Q_{\max}} = 1. \quad (8)$$

The induced flow rate, Q, is related to the pressure drop, ΔP, through the flow channel hydrodynamic resistance, R_h,

$$\Delta P = QR_h . \quad (9)$$

For a channel with a rectangular cross-section of height, h, width, w, and the

Lab on a Chip Accepted Manuscript

condition that $h > w$, the hydrodynamic resistance over the total channel pumping length L is given by [33,34]

$$R_h = \frac{12\mu L}{wh^3(1-0.63h/w)}. \quad (10)$$

Eqs. (6-9) can be combined to derive the linear pump curve for the net flow rate and applied voltage of an EO pump,

$$Q = -\frac{6wd\mu u_{EO}}{2wd^3R_h - 3\mu L_E}\Delta V. \quad (11)$$

2.2 Voltage Drop Across a PDMS Membrane

Contactless micro pumps share similar electro-osmotic principles with traditional EO pumps, however, the high resistive PDMS membrane serves to reduce the potential drop within the microchannel (ΔV) from that of the total potential applied (ΔV_{total}). We apply a simple electro-current model to determine the relationship between the potential applied and the potential within the microchannel. The electrical resistance, R, of the PDMS membrane is related to the material resistivity (ρ), the membrane length (L_m), and cross-section area (A), as $R = \left(\rho L_m / A\right)$. In the absence of counter ion screening at the PDMS membrane surface, the electrical resistance of each PDMS membrane (R_{PDMS}) and bulk fluid (R_{fluid}) are calculated based on the equation above. By Ohm's law, the effective voltage drop across the working fluid is

Lab on a Chip Accepted Manuscript

$$\Delta V = \Delta V_{total} \frac{R_{fluid}}{R_{total}}, \quad (12)$$

where $R_{total}=R_{PDMS} + R_{fluid}$.

When a DC voltage is dropped across the PDMS membrane, however, counter ions in the working electrolyte will accumulate at the PDMS-liquid interface, create an induced screening potential (ϕ_s) and reduce the magnitude of the electrostatic field in the main channel. The magnitude of this screening effect is a function to the applied electric field and counter ion concentration in the electrolyte solution. If the ion concentration is large enough, the applied field will be completely screened from the microchannel, and no electro-osmotic flow will be observed. If the applied voltage is large enough and able to exceed the screening potential, however, an electric field will penetrate into the bulk and impart an electro-osmotic slip velocity at the PDMS membrane surface.

A more general expression must take into account this screening potential, and link the total applied voltage to the voltage generated within the working flow channel,

$$\Delta V = \Delta V_{total} \frac{R_{fluid}}{R_{total}} - \phi_s . \quad (13)$$

Eq. (13) can be combined with Eqs. (6) and (11) to give relationships between the applied voltage, the maximum pump pressure, and the net flow rate. We will use these expressions to quantify pump performance for each given microfluidic geometry. In this work, we experimentally determine the screening potential from our experimental pump curves.

Lab on a Chip Accepted Manuscript

3. Materials and Methods

In this section, we describe the methods used to fabricate the microfluidic devices with integrated gallium metal electrodes, and how to operate these pumps with a high voltage external DC power supply.

3.1 Microfluidic Chip Fabrication

Each microfluidic pump consists of a flow channel, which is electrically isolated from four separate electrode channels by a thin PDMS membrane (Fig. 1a). The entire device was fabricated using common soft lithographic techniques. Briefly, microchannels were fabricated in PDMS (Momentive, RTV 615A). A 1:10 mixture of PDMS elastomer and curing agent was poured atop a lithographically fabricated SU-8 3050 (Microchem Corp.) polymer mold, cured and gently peeled off. Fluid ports were punched into the PDMS using a 0.75 mm biopsy punch (Ted Pella, Inc.). The microchannel and coverslip were exposed to oxygen plasma (Jelight, Model 42A), immediately aligned and sealed under an inverted microscope, and baked for 24 hours at 80 °C. This post-bond baking step improved the PDMS bond strength and prevented PDMS membrane leakage and rupture during pump operation. The completed device consisted of a main flow channel 300 μm wide and 50 μm high with four galium electrode channels 900 μm wide, each separated by a thin PDMS membrane, 45μm in thickness (Fig. 1b).

To fabricate each metal electrode, solid gallium metal was melted and injected into the side channels of the microdevice. Briefly, solid gallium metal (Sigma-Aldrich, 263265) and the PDMS chip were heated to 40 °C on a hot plate. With a melting temperature of 29.7 °C, the newly melted liquid gallium was loaded

Lab on a Chip Accepted Manuscript

into a 1 mL plastic syringe and immediately injected into the electrode side channels. Liquid gallium has a low viscosity (1.37mPa-s)[35] and therefore no PDMS surface treatment was required prior to injection. Electrical connection was made using 0.75 mm diameter copper wire leads inserted into each electrode injection hole. This method sealed the electrodes into each channel, and created an electrical connection for an external power source. With this fabrication process, multiple micropumps could be fabricated and utilized on a single microfluidic chip.

3.2 Reagents and Electrical Parameters

The pumping experiments were conducted using deionized water (DI). Silica particles and fluorescent dyes were used to image the induced electro-osmotic flow field and to quantify the fluid velocity. When using particles as flow tracers, 1.7 μm silica microparticles (Corpuscular Inc.) were diluted to 0.005% (w/v) in DI water. Zeta potential of the silica particles were measured to be -29.6 mV (Zetasizer , Malvern Instruments Ltd). Red and green fluorescent solutions were made by combining 100 μl stock solutions of Alexa Fluor 488 (green) and 594 (red) with 4 mL DI water. Both ionic fluorescent dyes and charged particle tracers can influence the electrical conductivity of the fluid, which could influence the accuracy of our theoretical calculations. Both ionic fluorescent dyes and charged particle tracers can influence the electrical conductivity of the fluid, which could influence the accuracy of our theoretical calculations. To take this into account, we based our pumping theory on the electrical conductivity of the fluorescent solutions and particle suspension used in this work. The electrical conductivity of fluorescent solutions and particle suspension used were 1 μS/cm and 2 μS/cm, respectively. The PDMS zeta potential used in our calculations was based on a low

Lab on a Chip Accepted Manuscript

conductivity buffer at neutral pH: -30 mV.[31]

3.3 PDMS Membrane Resistivity

The electrical resistivity of PDMS is needed to calculate the effective voltage drop across the main flow channel (Eq. 13) and is an important parameter in determining pump capability. The electrical resistivity of PDMS has been previously reported to be on the order of 10^{13} Ω-cm.[29] However, there is a wide range in reported values, and the electrical resistivity of a polymer can vary with temperature and mechanical stress.[36] After plasma bonding PDMS to a glass substrate and baking for 24 hours, we measured the resistivity of the PDMS membrane for each device using a high resistance ohmmeter (Alpha Labs Inc, Model HR2). The PDMS membrane resistivity in our loop device was 5.1×10^{10} Ω-cm and in the T-channel device it was 5.6×10^{10}. It is important to note, however, that we observed that PDMS post-bond baking time influences the PDMS resistivity. As baking time increases from 1 hour to more than 48 hours, the resistivity of PDMS membrane ascends from 10^{9} Ω-cm to 10^{13} Ω-cm, and approaches the reported value of PDMS resistivity.

Based on the measured fluid and PDMS resistivity, the resistance ratio given in Eq. (13), R_{fluid}/R_{total}, for the microfluidic loop and the T-channel used in this work were 1.2×10^{-3} and 2.2×10^{-3}, respectively.

3.4 Pump Operation

Each individual micropump was composed of four gallium electrodes, as shown in Fig 1a. To operate the pump, a high voltage power supply (PS325, Stanford Research System, CA) was wired to two separate electrode pairs – a

Lab on a Chip Accepted Manuscript

high positive voltage (V_1) was delivered to one pair, while the other two electrodes were connected to ground (V_2). When the power supply was activated the two pairs of electrodes served to created a uniform electric field down the flow channel, which induced electro-osmotic flow in the direction of the applied field. Reversing the polarity of the electrode array can therefore reverse the flow direction.

3.5 On-Chip Pump Control

To automate the activation and operation of each micropump, a LabVIEW based interface was established to achieve independent control of each pumping module. A 24 channel DIO USB controller (24R Elexol, Australia) was used to send user-controlled 5 volt digital signals to a customized 12 volt PCB driver board. Each 12 volt signal was then used to activate a series of high voltage relays (Cynergy, DAT70510) that were connected to the high voltage DC power supply (PS325, Stanford Research System, CA). When a 12 volt signal was delivered to the relay, a DC high voltage (.4 – 2.0 kV) was then delivered to a specific on-chip micropump.

4. Results and discussion

When a DC voltage was dropped across the metal electrodes, fluid flow was observed in the direction of the applied electric field. Pump quantification experiments were performed using two different microfluidic designs – a closed loop (Fig. 2a) and a T-channel (Fig. 2b) – in order to characterize the performance of the micropump under different hydrodynamic loading conditions.

Lab on a Chip Accepted Manuscript

4.1 Pump Characterization in a Closed Microfluidic Loop

First, experiments were performed on single pump within the microfluidic-closed loop with sealed inlet and outlet ports. In this microfluidic geometry, the back pressure within the loop is created by the pump, and the resulting flow rate is dictated by a combination of induced pump pressure and the microfluidic channel resistance, as described previously by Eq. (11). To quantify the total pump flow rate in terms of the applied voltage for a single device, flow experiments were performed using a single micro pump within the loop (Fig. 2a). Fluid velocity was tracked by measuring the trajectories of individual microparticle tracers suspended within the working fluid. Because the particles are negatively charged and exhibit electrophoresis in a DC field, we tracked particle motion on the opposing end of the loop to ensure that the electric field did not influence their motion. The fluid flow rate was calculated by equating the average fluid velocity with that of the channel cross-section area.

As is typical of traditional EO flow, shown in Fig.3, the experimentally measured flow rate is linearly proportional to the applied DC voltage. Unlike typical EO pumps, however, we observed an operational threshold voltage; below an applied voltage of 650 V no fluid motion was observed. We attribute this observation to double layer screening at the PDMS membrane surface. Because the DC electric field drives counter ion accumulation and the formation of an electric double layer at the microchannel sidewall, the electric field will be effectively screened from the main flow channel when the ion concentration is large enough to exceed the membrane surface potential. Above a critical value, however, there will not be enough counter ions in the bulk to screen the electric field and fluid flow will be observed.

Shown in Fig. 3, the flow rate in the loop varies linearly from 2 - 10 nL/min as

Lab on a Chip Accepted Manuscript

the applied potential increases from 1.2 kV to 2.3 kV. Using a screening potential of 650 V, the corresponding theoretical electro-osmotic flow rate from Eq. (11) is plotted against the experimental data in Fig. 3. As shown, the mathematical model provides an accurate prediction of pumping performance against hydrodynamic resistance within a closed microfluidic loop over a range of applied voltage (.65 – 2.3 kV).

4.2 Pump Characterization: The T-Junction Design

To measure pump pressure, experiments were performed at the channel junction within a microfluidic T-channel (Fig 2b). A micropump was fabricated within each of the channel inlets. Two solutions of deionized water were labeled with different colored fluorescent dyes, and each was then driven into separate fluid inlets with a constant pressure source. When the applied pressures were equal, a liquid interface was observed to form at the centerline within T-junction, shown in Fig. 2c. Similar to the microfluidic loop, the total flow rate in the main channel was determined by computing the average velocity of suspended particles trajectories, and multiplying by the microchannel cross-section area. Each of the two fluid inlet stream then comprised 50% of the total flow rate within the main channel. With each fluid inlet flow rate known, a single micro pump was activated to induce fluid flow in the direction opposing the externally applied pressure driven flow. The resulting EO-induced counter flow acted against the external flow field, and reduced the total flow rate within the microchannel. Under a critical voltage, the micro pump flow rate completely balanced the externally applied flow rate. The interface position became fixed at the entrance of the active pumping channel and flow from this fluidic channel ceased (Fig. 2d). Using Eq. 9, the experimentally determined flow rate was combined with the hydrodynamic resistance across the microchannel length (Eq. 10) to calculate the induced

Lab on a Chip Accepted Manuscript

pressure drop between pumping area and outlet, which was equal to the pressure drop created by the micro pump. This process was then repeated over a range of applied pressures. Therefore, using a microchannel T-junction we are able to experimentally measure the maximum output pressure of the micropump as a function of voltage. The resulting pump pressure vs. voltage dataset is shown in Fig. 4. The experimentally observed pumping pressure varies linearly from 16 Pa – 31 Pa for applied voltages ranging from 1.4 - 2.0 kV. Eq. (6) was used to predict pressure as a function of applied voltage. The theory is plotted in Fig. 4 and shows good agreement with our experimental data. For this microchannel geometry, the threshold operation voltage (screening potential) was experimentally determined to be 600 V.

4.3 Microfluidic Liquid Manipulation

We have presented two different microfluidic devices capable of quantifying the working performance of on-chip electrokinetic micro pumps. In this section we demonstrate the fluidic processing capability of these gallium pumps. Specifically, we present results showing their capacity to route fluid flow within a microchannel network and to create “plugs” of solute for fluid metering and on-chip electrophoresis applications.

4.3.1 Fluid Routing

The goal here is to demonstrate the ability to route fluid flow into a different path within the microfluidic network, and then deliver this flow to a specific outlet stream. To accomplish this objective, fluidic routing was performed using an open access microfluidic loop configuration with two inlets (IN1, IN2), three outlets (O1

Lab on a Chip Accepted Manuscript

– O3), and four integrated pumps (P1 – P4), as shown in Fig. 5. Each loop corner is highlighted with a dotted box and imaged to demonstrate fluid routing. IN1 and IN2 were used to deliver separate fluid streams, each labeled with a different fluorescent dye (colored green or red), using an external constant pressure source. The device was primed and allowed to reach steady state. When no pumps were active, the two solutions split evenly within the fluidic network; red buffer was driven to O1, green buffer was sent to O2, and a combination of two colors flowed out of O3 (Fig. 5b). To re-route flow, P1 was activated to work against the externally applied pressure. Shown in Fig. 5c, red colored fluid reverses direction and is driven into O1, while the green stream flows out of O3.

This experiment simulates a fluid delivery and control unit, which can be applied to LOC systems, like sequential sample injection, buffer delivery or product collection. By introducing programmable control to each pumping unit on-chip, the flow direction in each stream can become controllable and predictable in LOC systems. We are able to deliver target streams into specific outlets, which can potentially be used to alter the fluid network to discharge waste or for delivering user-defined amounts of washing buffer to different on-chip destinations. In the next section, we demonstrate the ability to use on-chip automated control with these micro pumps for microfluidic liquid metering.

4.3.2 On-Chip Sample Injection

There has been recent interest in developing microfluidic methods to deliver sample plugs for microchip capillary electrophoresis (MCE).[37] Traditional small sample injection strategies are classified into two categories, electrokinetic[38] and hydrodynamic.[39] Electrokinetic injection is the most commonly used technique in microchip capillary electrophoresis (MCE) due to its independence of an external

Lab on a Chip Accepted Manuscript

pressure source. The approach typically utilizes two different electro-osmotic fluid flows within a cross-shape microchannel device. First, EO flow is used to prime a sample solution across a single fluid channel. A second EO flow is then initiated perpendicular to the sample flow channel, which generates a small solute plug for further downstream analysis. Here, we demonstrate this process using a series of automated on-chip gallium-based micropumps. The plug generation device consists of a cross-shaped microchannel with three integrated on-chip micropumps (P1 – P3). The pumps are fabricated in each of the three arms of the cross, as shown in Fig. 6. The left-most fluid stream was primed with a green fluorescent buffer, which we interpret here as the sample solution, while a red dyed fluid filled the buffer channel. To generate a controlled plug of solute, we activated P1 to drive buffer down the channel while P2 and P3 were simultaneously switched on and off periodically using a series of computer controlled high voltage relays. This impulse loaded a sample plug into the buffer stream. Shown in Fig. 6b, the resulting off/on switching of the gallium micro pumps generates a series of solute plugs within the main flow channel. With the ability to automate the gallium micropump operation, this plug generator has the potential to serve as an upstream sample preparation unit for microfluidic capillary electrophoresis.

5. Conclusions

In conclusion, we have demonstrated a new metal-based contactless DC electro-osmotic micro pump capable of on-chip microfluidic pumping, routing and metering. The pump is driven by gallium metal electrodes integrated directly into the sidewalls of the flow channel, separated by a thin micron-scale PDMS membrane. The PDMS membrane serves as an insulating barrier and prevents

Lab on a Chip Accepted Manuscript

electrodes from being in direct contact with the working fluid. A high voltage (1.2 – 2.3 kV) DC electric field is utilized to overcome the induced ionic screening potential at the membrane, and drive a net fluid flow. The flow is electro-osmotic and scales linearly with the applied voltage. The maximum flow rates and pressures generated by the pump using DI water as a working buffer are 10 nL/min and 30 Pa, respectively. We measured the pump pressure and flow rate as a function of voltage using two different microfluidic geometries – a microfluidic loop and a T-shape channel. The resulting pump curves agree well with the presented electro-osmotic flow model. Finally, we demonstrate the ability for these micro pumps to route fluid flow and generate controlled plugs of solute within a microfluidic channel network.

One limitation of this current contactless design is the potential for low efficiency operation due to the electrically resistive PDMS membranes. These pumps also suffer from counter ion screening, which currently limits their use to low conductivity buffers. With our current design, the maximum operational conductivity where fluid flow is observed is 0.1 mS/cm. This number still falls below typical values associated with physiological buffers. Current research is underway on integrating conductive additives into the PDMS membranes in order to overcome these limitations.

Acknowledgements

We would like to thank Dr. Michael Sano and the research group of Dr. Rafael Davalos at Virginia Tech for helpful technical advice and discussion.

Lab on a Chip Accepted Manuscript

Figures

Figure 1.

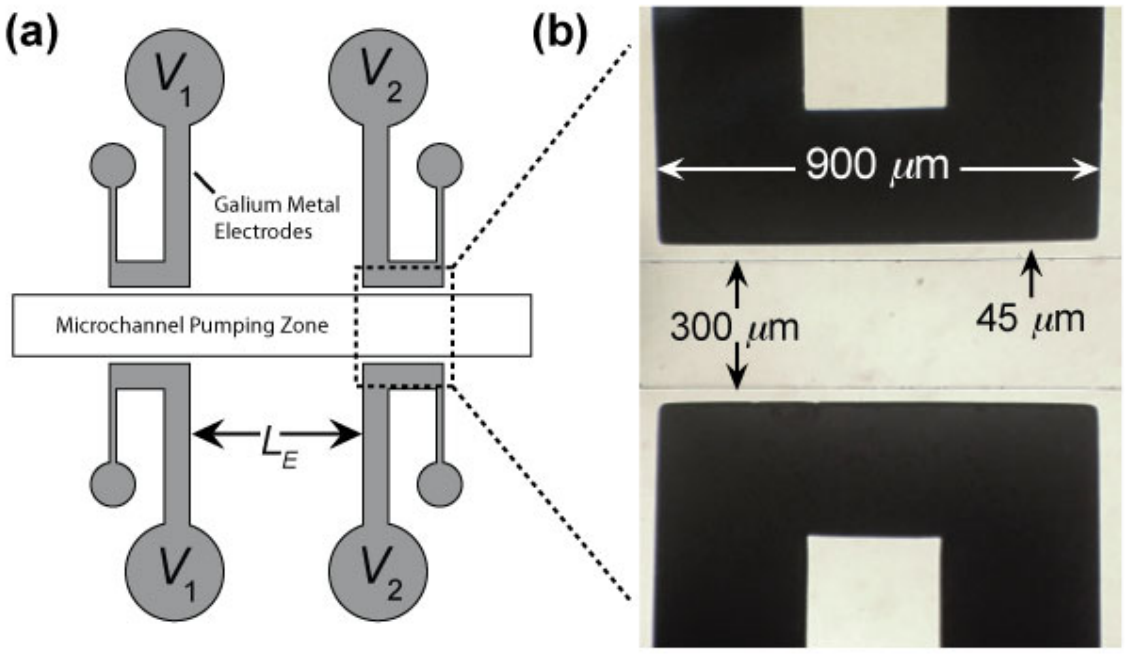

Figure 1. Schematic of a gallium metal contactless micropump. (a) A top view of a single pumping device. Each micropump contains four gallium electrodes separated from the microchannel by a thin PDMS membrane. (b) A micrograph of a pair of electrodes surrounding a microchannel. Each electrode is 900 μm wide, separated from the main channel by a 45 μm thick PDMS membrane.

Lab on a Chip Accepted Manuscript

Figure 2.

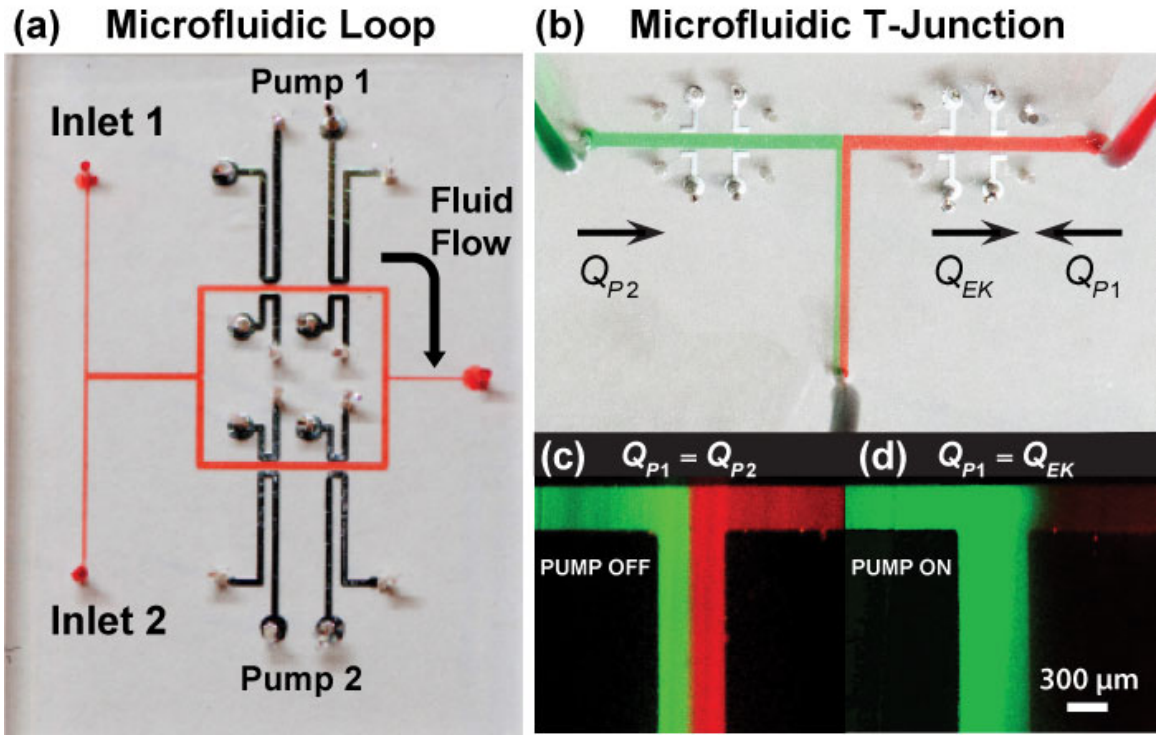

Figure 2. Microfluidic devices used to quantify the pumping flowrate vs voltage. (a) A microfluidic loop design with two integrated micropumps (1 and 2) is used to characterize pump performance under a fixed microchannel hydrodynamic resistance. (b) A microfluidic T-junction device is used to measure pump pressure under zero net flow rate. Two fluid streams are driven into the device using an external constant pressure source. (c) When the no pump is active and the flow rate of each stream is equal, the interface between the two fluid phases is centered within the main fluid channel. (d) The right-most pump is activated to completely cancel the pressure driven flow of the right-most fluid stream. When the pump flow rate is equal and opposite the pressure driven flow rate, the flow of this stream ceases and the interface position shifts towards the active pumping channel.

Lab on a Chip Accepted Manuscript

Figure 3.

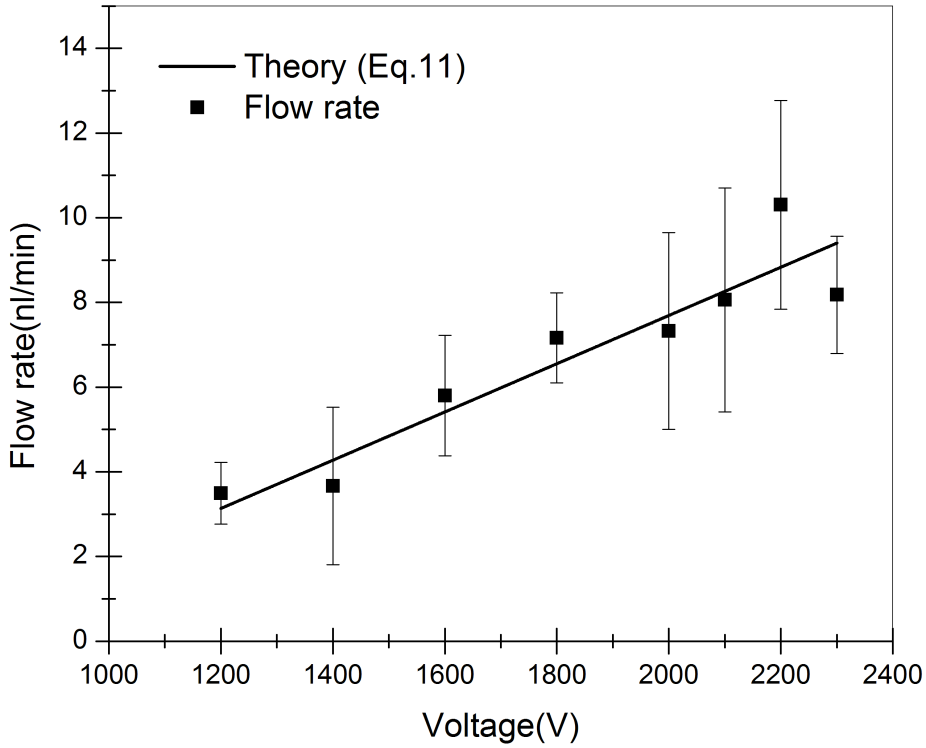

Figure 3. The microfluidic loop design was used to measure the micropump flow rate as a function of applied voltage under a known hydrodynamic resistance. The fluid flow rate varies linearly with the applied voltage and shows good agreement with the theoretical pump curve given by Eq. (11).

Lab on a Chip Accepted Manuscript

Figure 4.

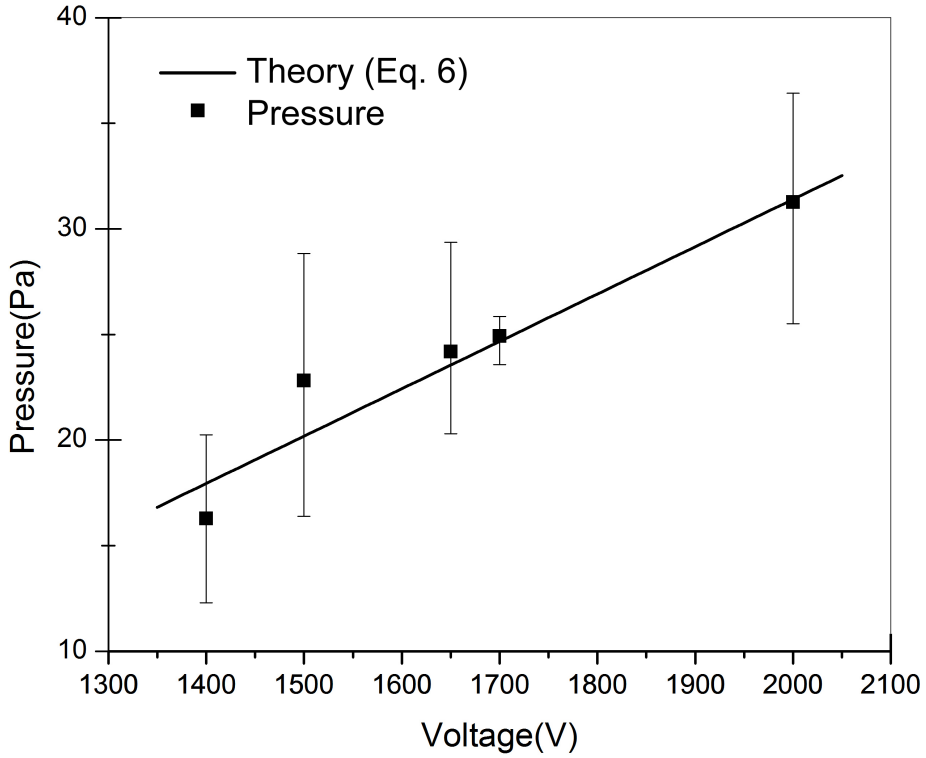

Figure 4. The T-junction was used to measure the maximum pressure generated by micropump when net fluid flow is ceased. The output pressure varies linearly with the applied voltage and matches the theoretical pump curve given by Eq. (6).

Lab on a Chip Accepted Manuscript

Figure 5.

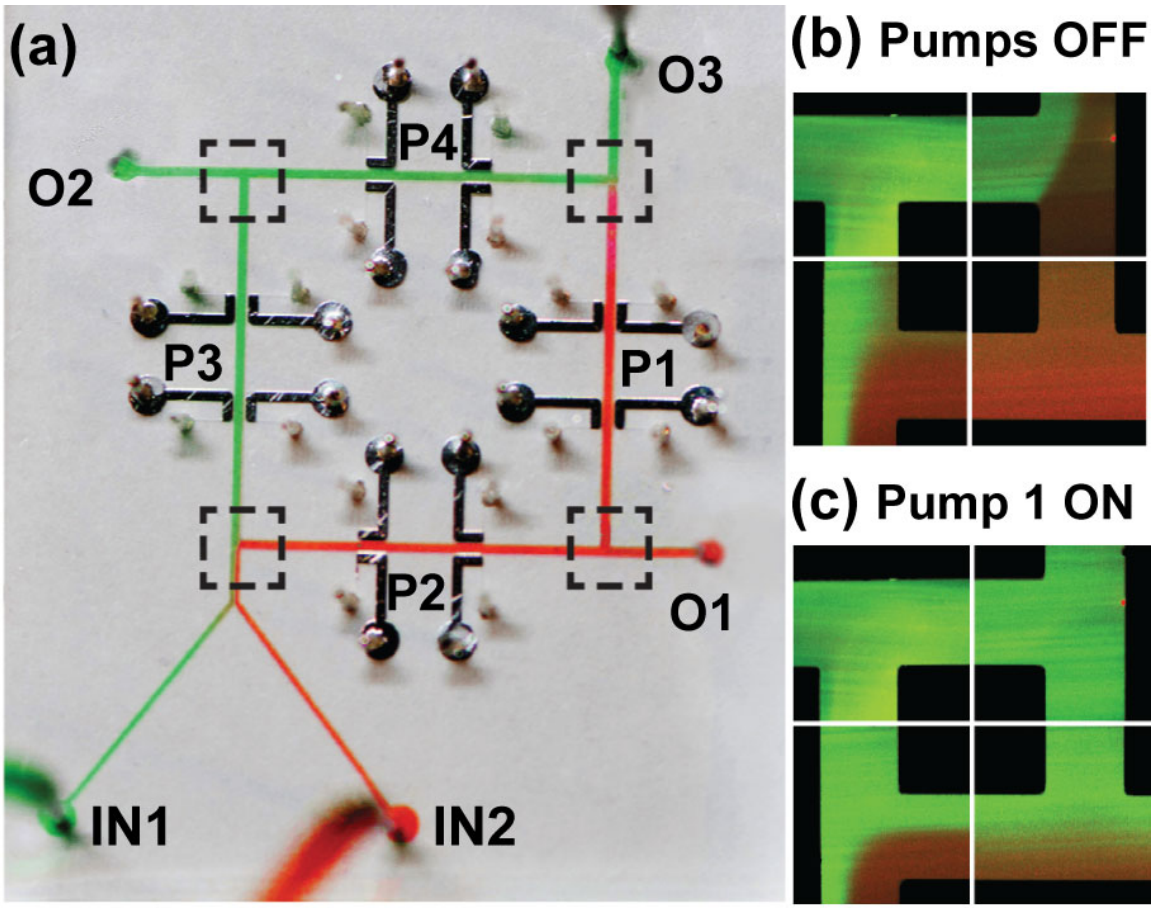

Figure 5. (a) A microfluidic loop with two inlets (IN1, IN2) and four integrated micropumps (P1-P4) is used to route fluid flow to different channel outlets (O1-O3). Each loop corner is highlighted with a dotted box and imaged to demonstrate fluid routing. (b) When no pumps are active fluid enters and exits the loop symmetrically. (c) The right-most pump is activated to eliminate the flow rate of red-dyed fluid at O3.

Lab on a Chip Accepted Manuscript

Figure 6.

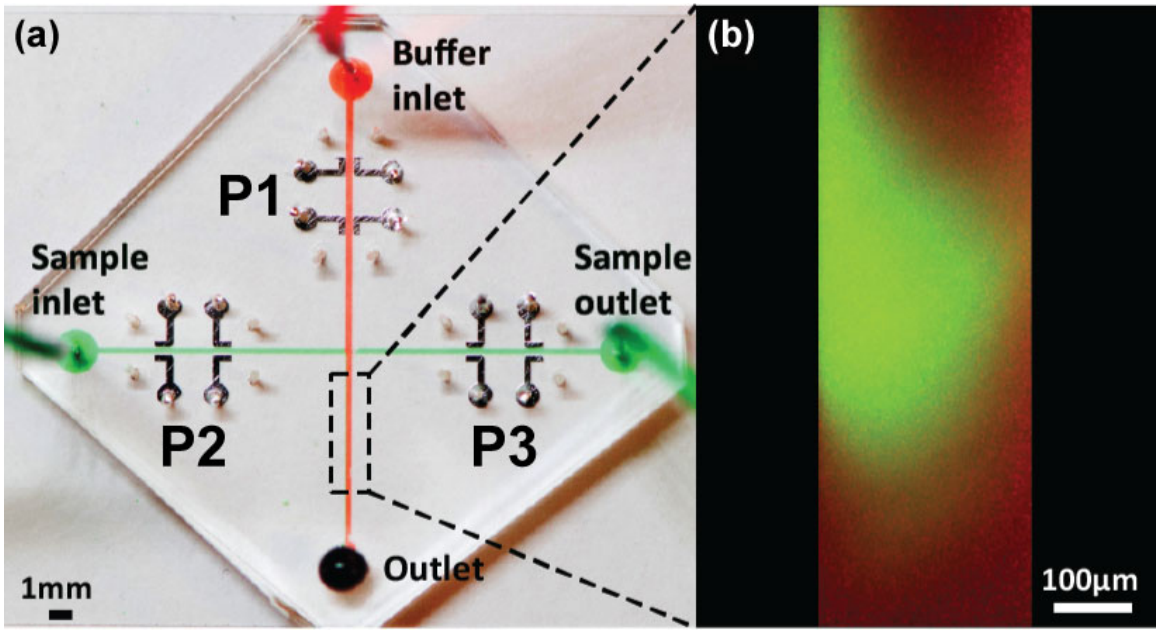

Figure 6. A cross-channel device with three integrated pumps (P1-P3) is used to generate plugs of solute. (a) Buffer is driven down a main channel from the channel inlet. Pumps P2 and P3 within the sample channel are pulsed on-off to generate a sample plug within the buffer channel.

Lab on a Chip Accepted Manuscript

References

1 S. J. Lee and S. Y. Lee, *Applied Microbiology & Biotechnology,* 2004, **64**, 289.

2 K. Seiler, Z. H. Fan, K. Fluri and D. J. Harrison, *Anal. Chem.,* 1994, **66**, 3485-3491.

3 J. G. Smits, *Sensors and Actuators A: Physical,* 1990, **21**, 203-206.

4 Friend,M.K.Tan and L.Y.Yeo and J.R., *EPL (Europhysics Letters),* 2009, **87**, 47003.

5 J. W. Kwon and E. S. Kim, *Sensors and Actuators A: Physical,* 2002, **97–98**, 729-733.

6 T. Thorsen, S. J. Maerkl and S. R. Quake, *Science,* 2002, **298**, 580-584.

7 R. Gorkin, J. Park, J. Siegrist, M. Amasia, B. S. Lee, J. Park, J. Kim, H. Kim, M. Madou and Y. Cho, *Lab Chip,* 2010, **10**, 1758-1773.

8 L. Y. Yeo and J. R. Friend, *Annu. Rev. Fluid Mech.,* 2014, **46**, 379-406.

9 C. L. Rice and R. Whitehead, *J. Phys. Chem.,* 1965, **69**, 4017-4024.

10 G. Garcia-Schwarz, A. Rogacs, S. S. Bahga and J. G. Santiago, *Journal Of Visualized Experiments: Jove,* 2012, , e3890.

11 M. O. A. Sommer and S. Larsen, *Journal of Synchrotron Radiation (Wiley-Blackwell),* 2005, **12**, 779.

12 K. N. Han, C. A. Li and G. H. Seong, *Annual Review of Analytical Chemistry,* 2013, **6**, 119-141.

13 Z. R. Gagnon, *Electrophoresis,* 2011, **32**, 2466.

14 C. B. Rohde, C. Gilleland, C. Samara and M. F. Yanik, *Life Science Systems and Applications Workshop, 2009. LiSSA 2009. IEEE/NIH,* 2009, , 52-55.

15 J. G. S. D J Laser and, *J Micromech Microengineering,* 2004, **14**, R35.

Lab on a Chip Accepted Manuscript

16 Brian D Iverson and Suresh,V.Garimella, *J Micromech Microengineering,* 2009, **19**, 055015.

17 P. Foroughi, Y. Zhao, J. Lawler and M. M. Ohadi, *AIP Conference Proceedings,* 2005, **746**, 46-54.

18 Z. Gagnon, J. Mazur and H. Chang, *Lab Chip,* 2010, **10**, 718-726.

19 J. C. T. Eijkel, C. Dalton, C. J. Hayden, J. P. H. Burt and A. Manz, *Sensors Actuators B: Chem.,* 2003, **92**, 215-221.

20 S. Pal, A. Datta, S. Sen, A. Mukhopdhyay, K. Bandopadhyay and R. Ganguly, *J Magn Magn Mater,* 2011, **323**, 2701-2709.

21 H. Moon, S. K. Cho, R. L. Garrell and C. ". J. Kim, *J. Appl. Phys.,* 2002, **92**, 4080.

22 Z. R. Gagnon and H. Chang, *Appl. Phys. Lett.,* 2009, **94**, 024101.

23 M. -. Nguyen, S. A. Grigoriev, A. A. Kalinnikov, A. A. Filippov, P. Millet and V. N. Fateev, *J. Appl. Electrochem.,* 2011, **41**, 1033-1042.

24 B. G. Hawkins and B. J. Kirby, *Electrophoresis,* 2010, **31**, 3622.

25 H. Moncada-Hernandez, J. L. Baylon-Cardiel, V. H. Pérez-González and B. H. Lapizco-Encinas, *Electrophoresis,* 2011, **32**, 2502.

26 A. Gencoglu, F. Camacho-Alanis, V. T. Nguyen, A. Nakano, A. Ros and A. R. Minerick, *Electrophoresis,* 2011, **32**, 2436-2447.

27 S. Sridharan, J. Zhu, G. Hu and X. Xuan, *Electrophoresis,* 2011, **32**, 2274.

28 J. P. Urbanski, T. Thorsen, J. A. Levitan and M. Z. Bazant, *Appl. Phys. Lett.,* 2006, **89**, 143508.

29 V. Studer, A. Pepin, Y. Chen and A. Ajdari, *Analyst,* 2004, **129**, 944-949.

30 M. Sano, R. Gallo-Villanueva, B. Lapizco-Encinas and R. Davalos, *Microfluidics and Nanofluidics,* 2013, 1-11.

31 P. Wang, Z. Chen and H. Chang, *Sensors & Actuators B: Chemical,* 2006, **113**, 500.

Lab on a Chip Accepted Manuscript

32 B. Kirby, *Micro- and nanoscale fluid mechanics : transport in microfluidic devices*, Cambridge University Press, New York, 2010.

33 J. Nguyen, Y. Wei, Y. Zheng, C. Wang and Y. Sun, *Lab Chip,* 2015, **15**, 1533-1544.

34 C. Morris and F. Forster, *Exp. Fluids,* 2004, **36**, 928-937.

35 M. J. Assael, I. J. Armyra, J. Brillo, S. V. Stankus, J. Wu and W. A. Wakeham, *J. Phys. Chem. Ref. Data,* 2012, **41**, 033101-16.

36 L. Wang, M. Zhang, M. Yang, W. Zhu, J. Wu, X. Gong and W. Wen, *Biomicrofluidics,* 2009, **3**, 034105.

37 L. Fu and C. Lin, *Anal. Chem.,* 2003, **75**, 5790-5796.

38 E. S. Roddy, H. Xu and A. G. Ewing, *Electrophoresis,* 2004, **25**, 229-242.

39 C. Lin, C. Chen, C. Lin and S. Chen, *Journal of Chromatography A,* 2004, **1051**, 69-74.

Lab on a Chip Accepted Manuscript

Table of Contents Entry

Contactless gallium metal electrodes, separated from microchannels by a micron-scale membrane, drive electro-osmotic micropumping, routing and fluidic metering.

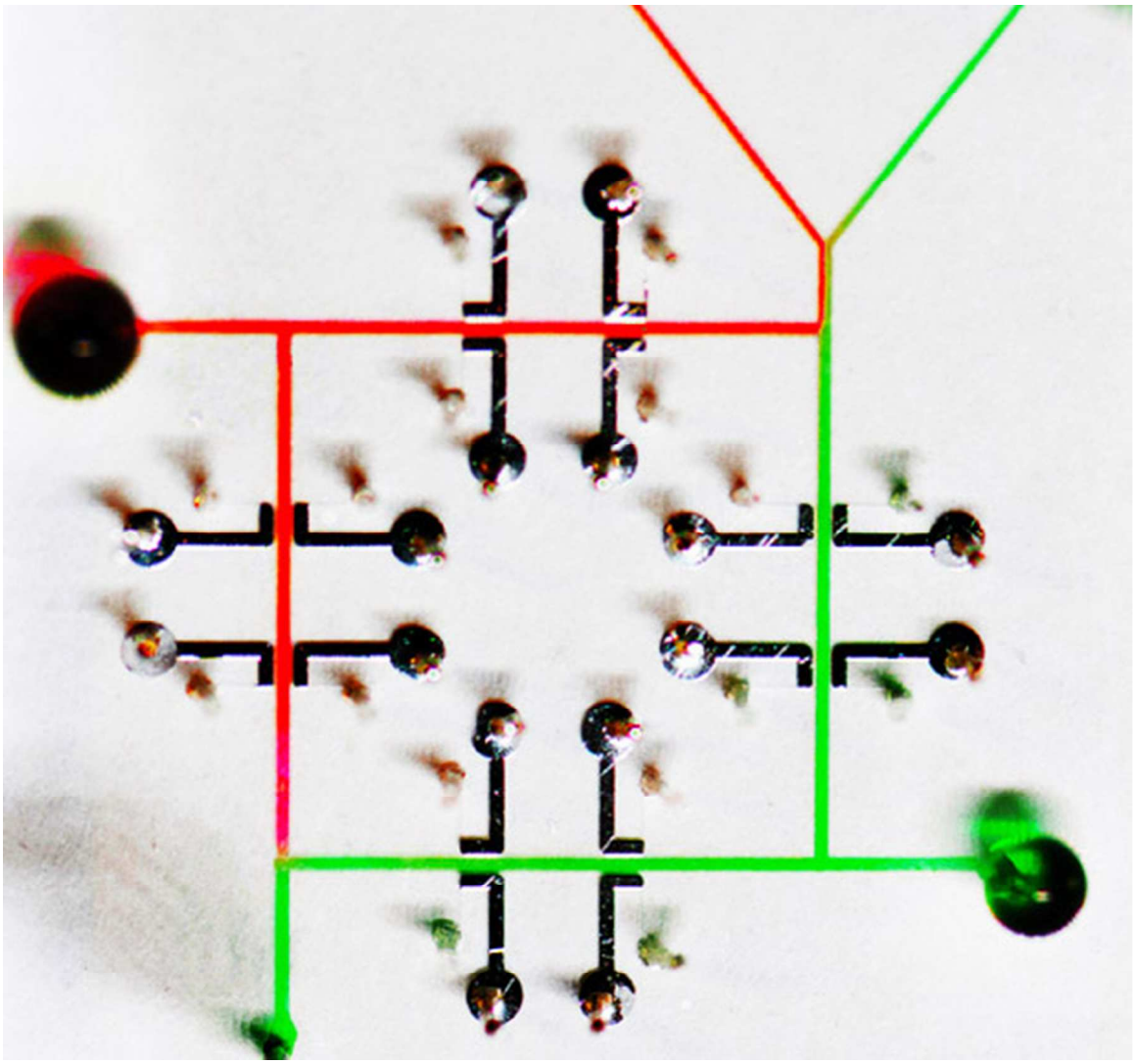

Lab on a Chip Accepted Manuscript